Magnetic polarons at finite temperature: One-hole spectroscopy study

Toni Guthardt,[1] Markus Scheb,[1] Jan von Delft,[1,2] Annabelle Bohrdt,[1,2,3] and Fabian Grusdt[1,2]
[1]*Department of Physics and Arnold Sommerfeld Center for Theoretical Physics (ASC), Ludwig-Maximilians-University Munich, Theresienstrasse 37, D-80333 Munich, Germany*
[2]*Munich Center for Quantum Science and Technology, Schellingstrasse 4, D-80799 Munich, Germany*
[3]*Institut für Theoretische Physik, Universität Regensburg, D-93035 Regensburg, Germany*

(Received 14 April 2025; revised 24 September 2025; accepted 7 October 2025; published 14 November 2025)

The physics of strongly correlated fermions described by Hubbard or t-J models in the underdoped regime—relevant for high-temperature superconductivity in cuprate compounds—remains a subject of ongoing debate. In particular, the nature of charge carriers in this regime is poorly understood, in part due to the unusual properties of their spectral function. In this Letter, we present unbiased numerical results for the one-hole spectral function in a t-J model at finite temperatures. Our study provides valuable insights into the underlying physics of magnetic (or spin-) polaron formation in a doped antiferromagnet (AFM). For example, we find how the suppression of spectral weight outside the magnetic Brillouin zone—a precursor of Fermi arc formation–disappears with increasing temperature, revealing nearly-deconfined spinon excitations of the undoped AFM. The pristine setting we consider can be directly explored using quantum simulators. Our calculations demonstrate that coherent quasiparticle peaks associated with magnetic polarons can be observed up to temperatures $T > J$ above the spin-exchange J, routinely obtained in such experiments. This paves the way for future studies of the fate of magnetic polarons in the pseudogap phase.

DOI: 10.1103/4588-hpc2

I. INTRODUCTION

The disappearance of antiferromagnetism underlies a variety of exotic phenomena of strongly correlated electrons, including heavy-fermion superconductivity related to Kondo couplings [1], or pseudogap formation in hole-doped cuprate compounds [2,3]. A natural starting point for understanding the underlying physics is to work in the strong-coupling limit, where Hubbard interactions $U \gg t$ dominate over tunneling t, and consider the elementary charge carriers of the doped AFM Mott insulator. These magnetic, or spin-, polarons [4–7] correspond to the quasiparticles formed upon removing a single fermion from the Mott insulator and creating a mobile vacancy, the doped hole. They have been observed experimentally in solids [8,9] and in neutral atom quantum simulators [10–12].

Angle-resolved photoemission spectroscopy [13] (ARPES) studies on hole-doped cuprates provide evidence that the physics of magnetic polarons, whose ground states are well understood deep in the AFM phase [6,7,14–22], is related to the physics of Fermi arcs in the pseudogap regime. Specifically, laser-ARPES studies on few-layer copper-oxide compounds suggest that the small Fermi pockets around the nodal point $(\pi/2, \pi/2)$ associated with magnetic polarons continuously evolves into Fermi arcs with decreasing spectral weight outside the magnetic Brillouin zone (BZ) as doping is increased from 1% to around 5% [23]. This is consistent with theoretical calculations based on linear spin-wave theory [24] and cellular dynamical mean-field theory [25], and motivates further studies of the distribution of spectral weight of magnetic polarons.

In this Letter, we present results from unbiased numerical simulations of the one-hole spectral function in the t-J model at variable temperatures, based on matrix product states (MPS) [26–28]. First we reveal stable magnetic polaron features in the spectrum up to temperatures $T > J$ well above the spin-exchange J, see Fig. 1. This is remarkable, given the quick demise of AFM correlations beyond nearest neighbor sites at these high temperatures. Second, when temperature is increased we report on the appearance of low-energy spectral weight outside the magnetic BZ, where the signal is strongly suppressed at low temperatures in a precursor of Fermi-arc formation. We explain these features in terms of thermally excited, nearly-deconfined spinons [29] in the parent AFM.

The spectral properties of magnetic polarons in the t-J model have been investigated in great detail at $T = 0$ [30–33]. Initial work was based on the linear-spin wave approximation [6,7], and combined with the self-consistent Born approximation (SCBA) to predict the shape of the one-hole spectrum [16,18,34–36]. While the SCBA has been validated on the level of the linear spin-wave Hamiltonian [37], unbiased numerical studies of the one-hole spectrum in the more fundamental t-J model, including exact diagonalization [38,39], diagrammatic Monte Carlo [40,41] and MPS [42], have revealed discrepancies at higher energies. These have been traced back to interactions among spin-waves [22,43],

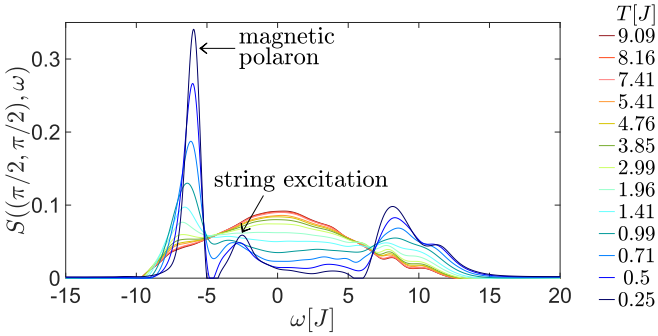

FIG. 1. Single-hole ARPES spectrum at the nodal point $\mathbf{k} = (\pi/2, \pi/2)$, computed for various temperatures T indicated on the right. We consider a t-J model at $t/J = 3$, on a four-leg cylinder accessible to our time-dependent MPS simulations that we combine with purification schemes to obtain finite-T spectra. At low energies, around $\omega \lesssim -6J$, a well-defined quasiparticle peak associated with magnetic polaron formation is visible up to fairly high temperatures ($T \simeq 1.4J$).

which lead to the disappearance of string-excitations of magnetic polarons [4,35,44–47] beyond the first vibrational peak [41,42]. The finite-temperature one-hole spectrum remains much less studied, with the notable exception of a linear-spin wave analysis [48].

One of the most intriguing features of the $T = 0$ one-hole spectrum, not captured by SCBA, is a strong suppression of spectral weight outside the magnetic BZ up to energies on the order of t above the ground state when $t > J$ [40,42]. This phenomenon has been argued [42] to be related to the formation of Fermi-arcs, through features in the spectrum associated with nearly-deconfined spinons. Our analysis of finite temperature spectra in this Letter provides direct evidence for this picture.

While the temperatures studied in this manuscript may appear high from the perspective of low-temperature condensed matter physics, the regime $T = 0.25$–$2J$ is directly relevant for several reasons. First, such temperatures are routinely accessed in quantum simulation platforms, including ultracold atoms in optical lattices and Rydberg atom arrays, which serve as tunable models of doped Mott insulators. Even in solid-state systems like the cuprates, angle-resolved photoemission spectroscopy (ARPES) is typically performed at finite temperature, with $T \approx 0.25J$ corresponding to room temperature. Second, our finding that spin polaron features remain well defined up to $T \sim 2J$ highlights their robustness beyond the zero-temperature limit, suggesting that magnetic polarons are relevant for the finite-temperature behavior of strongly correlated systems.

II. MODEL AND METHOD

Throughout this work we consider zero or one hole in the t-J Hamiltonian,

$$\hat{H} = -t \sum_{\langle \mathbf{i},\mathbf{j}\rangle,\sigma} \hat{\mathcal{P}}(\hat{c}^{\dagger}_{\mathbf{i},\sigma}\hat{c}_{\mathbf{j},\sigma} + \text{H.c.})\hat{\mathcal{P}} + J \sum_{\langle \mathbf{i},\mathbf{j}\rangle} \left(\hat{\mathbf{S}}_{\mathbf{i}} \cdot \hat{\mathbf{S}}_{\mathbf{j}} - \frac{\hat{n}_{\mathbf{i}}\hat{n}_{\mathbf{j}}}{4}\right), \tag{1}$$

where $\hat{\mathcal{P}}$ projects onto states with at most one fermion $\hat{c}_{\mathbf{j},\sigma}$ per site, i.e., $\hat{n}_{\mathbf{j}} = \sum_{\sigma} \hat{c}^{\dagger}_{\mathbf{j},\sigma}\hat{c}_{\mathbf{j},\sigma} \leqslant 1$, and $\hat{\mathbf{S}}_{\mathbf{j}}$ is the spin operator at site $\mathbf{j}$. This model has been proposed to describe high-T_c cuprate superconductors [49], captures key properties of their phase diagrams [50] and can be obtained, up to a correlated hole-hopping term $\propto J = 4t^2/U$, as the low-energy limit of the Hubbard model.

In addition to their (approximate) realizations in solids, pristine implementations of t-J [12,51–53] and Fermi-Hubbard models [54–56] with tunable model parameters have been achieved in neutral atom quantum simulators, as well as in digital platforms [57,58]. In all of these experimental settings, the momentum-resolved spectral function that we study in this Letter can be measured, using ARPES in solids or neutral-atom incarnations of the latter in quantum simulators [52,59–64].

We calculate the one-hole spectral function, $S(\mathbf{k}, \omega) = -\Im A(\mathbf{k}, \omega)/\pi$, from the Fourier transformation,

$$A(\mathbf{k}, \omega) = \int_{-\infty}^{\infty} d\tau\ \mathrm{e}^{-\mathrm{i}\omega\tau} \sum_{\mathbf{j}} \mathrm{e}^{-\mathrm{i}\mathbf{k}\mathbf{j}} C_{\mathbf{0},\mathbf{j}}(\tau), \tag{2}$$

of a space and time-dependent correlation function $C_{\mathbf{i},\mathbf{j}}(\tau)$. The latter can be directly computed using MPS as the time-evolution of an initial thermal state of the AFM with a single hole created at site $\mathbf{i}$ (we set $\hbar = 1$),

$$C_{\mathbf{i},\mathbf{j}}(\tau) = -\mathrm{i} \sum_{\sigma} \langle \psi^{\text{puri}}_{\text{equil}} | \mathrm{e}^{\mathrm{i}\hat{H}\tau} \hat{c}^{\dagger}_{\mathbf{j},\sigma} \mathrm{e}^{-\mathrm{i}\hat{H}\tau} \hat{c}_{\mathbf{i},\sigma} | \psi^{\text{puri}}_{\text{equil}} \rangle. \tag{3}$$

Here $|\psi^{\text{puri}}_{\text{equil}}\rangle$ is the finite temperature purified state of the undoped AFM in equilibrium.

Our simulations start by calculating $|\psi^{\text{puri}}_{\text{equil}}\rangle$ on a cylinder with length $L_x = 18$ and width $L_y = 4$. We use the density matrix renormalization group [65,66] in the language of MPS [67], adapted to finite temperatures via a purification scheme [68–70] and enhanced by the use of disentanglers [26]. We simulate the time-evolution in Eq. (3) by combining two MPS-based algorithms [27]: To capture the initial spreading of entanglement across the MPS we begin with a single step of the more expensive, global Krylov scheme [71–73]. Then we switch to the local, but less expensive time-dependent-variational-principle algorithm [74,75]. This procedure is improved by the use of a backwards-time-evolution scheme [76–78], which allows to reach longer times without further approximations. In addition, we make use of controlled bond expansion [28,79], which effectively performs two-site optimization at one-site cost. Symmetries in tensor network computations were exploited using the QSpace tensor library [80–82]. Finally, in order to extend the time window that we can use for the integration in Eq. (2), we employ linear prediction [83] and multiply the correlation function $C_{\mathbf{0},\mathbf{j}}(t)$ with a Gaussian envelope [84].

While density matrix renormalization group (DMRG) methods are most efficient in one dimension, recent algorithmic developments have significantly extended their applicability to quasi-two-dimensional systems. In particular, modern tensor network techniques such as the controlled bond expansion (CBE) allow for reliable simulations of challenging quasi-two-dimensional systems. These advances enable us to

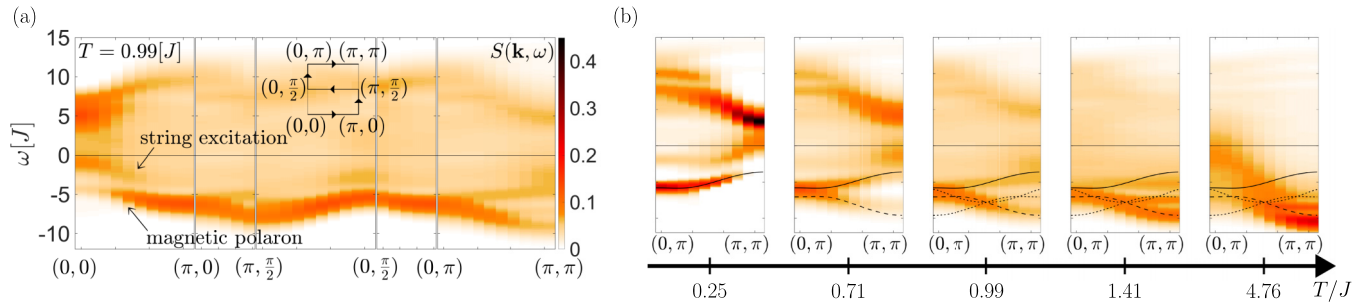

FIG. 2. Finite temperature ARPES spectra, computed for $t/J = 3$ on a four-leg cylinder. We use the convention $\omega > 0$ for positive energy excitations. Note that this is opposite to the convention commonly adopted in ARPES, where $\omega < 0$ corresponds to occupied states. (a) We show the single-hole spectrum at $T = 0.99\,J$ along the S-shaped cut through the BZ shown in the inset. At low energies the characteristic spectral signatures of magnetic polarons remain visible. (b) We show the evolution of the spectrum as temperature T/J is increased, along a cut from $(0,\pi)$ to (π,π). Around (π,π), a pronounced spectral gap for $\omega \lesssim 0$ is visible at the lowest temperatures which gradually fills up as T is increased. The predicted low-energy thermal spinon lines (dashed and dotted lines) for this four-leg cylinder are also indicated, along with the approximate magnetic polaron dispersion (solid lines), as discussed in the main text.

access intrinsic spectral features of the two-dimensional t-J model with state-of-the-art accuracy.

An additional challenge arises from ensuring sufficient thermalization during real-time evolution at finite temperature. Since entanglement grows rapidly and the Hilbert space is truncated, there is a risk that incomplete thermalization could artificially enhance coherent features. To mitigate this, we perform convergence checks with respect to several parameters including the bond dimension, see Supplemental Material [85], ensuring that the extracted spectral features are robust and physically meaningful.

A. Quasiparticle properties at finite T

We begin the discussion of our results by focusing on the quasiparticle peak associated with the formation of a magnetic polaron. Figure 1 shows spectral cuts $S(\mathbf{k},\omega)$ for different temperatures at the nodal point, $\mathbf{k} = (\pi/2, \pi/2)$, where the minimum of the magnetic polaron dispersion is located. We consider the case $t/J = 3$, but obtain similar results for $t/J = 1$ and 5, see Supplemental Material [85]. For the lowest temperatures, $T = 0.25\,J$, we observe a sharp quasiparticle peak around $\omega \approx -6\,J$ whose width is Fourier-limited by the finite time of our accessible time-dependent MPS calculations of Eq. (3).

With increasing temperature, up to $T \lesssim 2\,J$, the magnetic polaron peak remains clearly visible. In this regime its energy shifts to lower frequency, reaching $\omega \approx -7\,J$ at $T \approx 2\,J$. Moreover the peak broadens and its width is temperature- instead of Fourier-limited. This behavior is typical for polaronic models, independent of the details of the model [86]. At temperatures above $T \gtrsim 2\,J$, the coherent quasiparticle feature disappears, making way for a low-energy shoulder which finally also dissolves above $T \gtrsim 5\,J$. At that point, the entire spectrum becomes featureless and broad. The associated energy scale is consistent with the magnetic polaron bandwidth of $W \approx 2\,J$ [16,19,20]. Similar behavior is found at other momenta within the magnetic BZ, see Fig. 2(a).

For the lowest temperatures the first string excitation peak of the polaron [40–42,46], at $\Delta\omega \approx 3.5\,J$ above the ground state, is also clearly visible in Fig. 1. Like the main quasiparticle peak, this feature broadens and shifts to lower frequencies before it vanishes at temperatures $T \approx J$, somewhat before the magnetic polaron ground state disappears. Closer to the center of the BZ around $\mathbf{k} = (0,0)$, this first string excitation remains visible up to slightly higher temperatures, see Fig. 2(a).

The robustness of the magnetic polaron features that we find upon increasing temperature to between J and $2\,J$ is remarkable, given that the undoped parent AFM in two dimensions has no long-range order at any $T > 0$. The AFM correlation length diverges exponentially with $1/T$ and reaches a few lattice sites only below $T \lesssim 0.6\,J$ [87]. On the other hand, the nearest-neighbor spin-spin correlations of the parent AFM become sizable already around $T \lesssim J$. This suggests that the presence of local spin correlations is essential for seeing spectral signatures of magnetic polarons, rather than long-range AFM order.

B. Low-energy spectral weight

Next we discuss the evolution of low-energy spectral weight around $\mathbf{k} = (\pi,\pi)$ outside the magnetic BZ as temperature is increased. Our numerical results are shown in Fig. 2(b), focusing on a cut from $(0,\pi)$ to (π,π), where the redistribution of low-energy spectral weight is most pronounced. In agreement with calculations at $T = 0$ [42], at low temperatures $T \ll J$ we observe a nearly complete suppression of spectral weight below $\omega \lesssim 0$ at $\mathbf{k} = (\pi,\pi)$. Since the undoped parent AFM ground state breaks the translational symmetry, single-hole eigenstates at $\mathbf{k} = (\pi,\pi)$ exist at the same eigenenergies as at $\mathbf{k} = (0,0)$, where spectral weight is observed down to $\omega_{\mathrm{min}} \approx -t$. That is, all magnetic polaron states at $\mathbf{k} = (\pi,\pi)$ with energies below $\mathcal{O}(t)$ above the ground state have negligible spectral weight. We confirm this picture by our calculations of the one-hole spectrum at $t/J = 5$, see Supplemental Material [85], where an even larger spectral gap $\approx 10\,J$ is found at $\mathbf{k} = (\pi,\pi)$ at low temperature.

This behavior can be interpreted [42] as a precursor of Fermi-arc formation observed in hole-doped cuprates in the pseudogap regime, where a sharp drop of spectral weight across the edge of the magnetic BZ is found [23,88]. A similar

feature is well known to arise in the one-hole spectrum of a one-dimensional (1D) spin-chain [89], where it is explained by a combination of spin-charge separation and the description of the one-dimensional Heisenberg AFM as a spinon Fermi sea [90–92]. However, exact numerical studies in 1D systems found that this feature disappears upon increasing temperature [63], which can be traced back to thermal excitations of spinon states above the spinon Fermi surface [63,93]. Now we report on a similar effect in two-dimensional systems.

Upon increasing temperature beyond $T \gtrsim 0.7J$, in Fig. 2(b) we indeed observe the gradual reemergence of low-energy spectral weight at $\mathbf{k} = (\pi, \pi)$. On the one hand, the magnetic polaron branch featuring a dispersion maximum at $\mathbf{k} = (\pi, \pi)$ [solid lines in Fig. 2(b)] gains spectral weight and remains visible as a well-defined peak beyond $T \gtrsim 1.4J$, before thermal broadening dominates above $T > 2J$. On the other hand, additional weight appears below the magnetic polaron branch, down to frequencies well below the lowest spectral feature at $T = 0$ [42] located at $\mathbf{k} = (\pi/2, \pi/2)$. This indicates that the underlying microscopic processes extract energy from thermal excitations on top of the undoped initial state. At $T \gg J$ the lowest-energy spectral feature we find across the entire BZ is located at $\mathbf{k} = (\pi, \pi)$, which motivates us to study this momentum point more closely.

While our analysis focuses on the $(0, \pi)$–(π, π) direction, we have also examined other momentum cuts, such as $(\pi, 0)$–(π, π), which display qualitatively similar trends. This suggests that the observed redistribution of low-energy spectral weight across the magnetic Brillouin zone is a robust feature, even though a full momentum-resolved analysis is limited by resolution and computational cost.

Interestingly, the reappearance of spectral weight near (π, π) at elevated temperatures resembles features reported in lightly doped systems [94,95], suggesting a connection between thermal and doping-induced excitations. This similarity may reflect the mixing of particle and hole contributions at finite temperature, as expected from the Lehmann representation, where thermally excited spin backgrounds can enable processes analogous to those in doped systems. Such parallels highlight the broader relevance of our findings across different regimes of strongly correlated matter.

The additional spectral weight appearing around $\mathbf{k} = (\pi, \pi)$ as temperature is increased has a notable sub-structure. First, at $T = 0.71J$ in Fig. 2(b), we observe one additional low-energy branch emerging $\mathcal{O}(J)$ below the magnetic polaron (following the dashed line). Later, beyond $T \geqslant 0.99J$ in Fig. 2(b), a further pronounced maximum emerges between the two previous lines around $\mathbf{k} = (\pi, \pi)$, which remains visible up to high temperatures $T > 4J$. The same phenomenology, with two additional branches emerging at two different temperatures, is found in our simulations at $t/J = 5$, see Supplemental Material [85]. In particular, a comparison of the additional branches at $t/J = 3$ and 5 shows that their energy scales as $\propto J$, almost completely independent of t/J in the regime where $t > J$, see Supplemental Material [85] for details.

We expect that the existence of such well-defined peaks in the spectrum, appearing at elevated temperatures, is likely related to the small circumference, $L_y = 4$, of the cylinder to which our simulations are constrained due to technical limitations. This view is supported by our following theoretical interpretation, and suggests that a less structured spectral feature with a width of several J can be expected below a well-defined magnetic polaron branch in an extended two-dimensional system.

C. Nearly-deconfined spinons

To explain the low-energy spectral features emerging around $\mathbf{k} = (\pi, \pi)$ at intermediate temperatures, $0.5J \lesssim T \lesssim 2J$, we model the undoped parent AFM as a resonating valence-bond (RVB) state perturbed by a staggered magnetic field representing the nonzero Néel order parameter of the AFM ground state [29,96]. To this end, spin operators are represented by fermionic spinons $\hat{f}_{\mathbf{j},\alpha}$ in the following way, $\hat{\mathbf{S}}^{\mu}_{\mathbf{j}} = \frac{1}{2}\sum_{\alpha,\beta=\uparrow,\downarrow} \hat{f}^{\dagger}_{\mathbf{j},\alpha}\sigma^{\mu}_{\alpha,\beta}\hat{f}_{\mathbf{j},\beta}$, where σ^{μ} denotes Pauli matrices ($\mu = x, y, z$) and subject to the constraint $\sum_{\alpha} \hat{f}^{\dagger}_{\mathbf{j},\alpha}\hat{f}_{\mathbf{j},\alpha} = 1$. A mean-field Hamiltonian for spinons yielding accurate ground state energies (below 1% error) after Gutzwiller projection [29,96,97] includes a staggered magnetic flux $\pm\Phi$ and a staggered magnetic field B_{st} breaking the SU(2) symmetry. It leads to a two-band spinon dispersion $\omega^{\pm}_{\mathrm{s}}(\mathbf{k})$ for $\mathbf{k}$ in the magnetic BZ, with bandwidth $\mathcal{O}(J)$, of which the lower band $\omega^{-}_{\mathrm{s}}(\mathbf{k}) < 0$ is filled and the upper band $\omega^{+}_{\mathrm{s}}(\mathbf{k}) = -\omega^{-}_{\mathrm{s}}(\mathbf{k})$ is empty.

The antiferromagnetic pinning field $B_{\mathrm{st}} \approx 0.44J$ introduced in the RVB mean-field ansatz is a variational parameter used to model short-range AFM correlations. While it explicitly breaks SU(2) symmetry at the mean-field level, it does not artificially cause the suppression of spectral weight at (π, π). Similar suppression is found even for $B_{\mathrm{st}} = 0$ [42] and only disappears for significantly larger pinning strengths. As temperature increases, the effective B_{st} decreases and vanishes in the high-temperature regime [98], consistent with the absence of long-range magnetic order.

While spinons are confined in the parent AFM, appearing as spin-one pairs (magnons) in the dynamical structure factor, their nearly-deconfined nature has been argued to manifest in high-energy spin-excitations indirectly revealing the structure of weakly interacting spinons [29]. In addition, it has been shown that individual doped holes $\hat{c}_{\sigma} \sim \hat{f}_{\sigma}\hat{h}^{\dagger}$ can be described as bound states of confined chargons $\hat{h}$ and spinons [20]. Since chargons are light (mass $\propto 1/t$) and spinons heavy (mass $\propto 1/J$), the dispersion relation of the resulting magnetic polaron is essentially determined by $-\omega^{-}_{\mathrm{s}}(\mathbf{k}) = \omega^{+}_{\mathrm{s}}(\mathbf{k})$ up to an overall normalization [19]. Inspection of the spinon dispersion $\omega^{\pm}_{\mathrm{s}}(\mathbf{k})$, see Supplemental Material [85], reveals that this picture correctly reproduces the shape of the magnetic polaron dispersion $\omega_{\mathrm{mp}}(\mathbf{k})$ [20], as confirmed by our fit to the polaron branch in Fig. 2(b). This picture moreover explains the drop of spectral weight outside the magnetic BZ at low temperatures, see Fig. 3(a), since the spinon Fermi sea essentially extends to the edge of the magnetic BZ [42].

It should be noted that our mean-field approach is based on a slave-fermion decomposition with a fixed mean-field gauge choice, in which the spinon momentum coincides with the physical electron momentum. While the parton construction introduces an internal gauge redundancy, gauge fluctuations are neglected at the mean-field level. In this regime, the spinon largely determines the low-energy structure of the magnetic

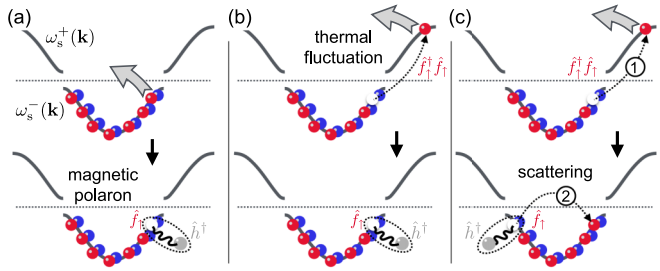

FIG. 3. Illustration of spinon states contributing to the single-hole ARPES spectrum. Initial states (top row) connected to final states (bottom row) by $\hat{c}_\sigma = \hat{f}_\sigma \hat{h}^\dagger$ are shown. (a) At $T = 0$ a spinon from the lower band is removed and a spinon-chargon ($\hat{f}\hat{h}^\dagger$) bound state constituting the magnetic polaron is formed. (b) At $T > 0$, thermal fluctuations lead to spinons in the upper band which can be deexcited by the ARPES beam. (c) Combining scenario (b) with an additional scattering of the spinon-hole $\hat{f}$ off the chargon $\hat{h}^\dagger$ leads to additional spectral features.

polaron, while the chargon contributes a broad background. This justifies using the spinon dispersion $\omega_s^-(\mathbf{k})$ as a proxy for the dispersion relation of the magnetic polaron.

Also note that although the holon is light and moves rapidly for $t \gg J$, the low-energy part of the spectral function is governed by the spinon due to its larger effective mass. In the magnetic polaron picture, the spinon-holon bound state inherits its dispersion primarily from the heavier spinon component, leading to $\omega_{\mathrm{mp}}(\mathbf{k}) \approx \omega_s^-(\mathbf{k})$. While the holon perturbs the spin background, this dressing process does not destroy spinon coherence but instead renormalizes it, giving rise to a well-defined quasiparticle with internal spinon structure. The use of a mean-field RVB background remains justified in this regime due to the persistence of antiferromagnetic correlations and the coherence of spinon dynamics.

If a thermally excited spinon $\hat{f}^\dagger_{\mathbf{k}}$ in the upper band, corresponding to $\mathbf{k}$ outside the magnetic BZ [42], exists in the initial state and is deexcited by the ARPES beam, the remaining $\hat{f}_{\mathbf{k}'}$ hole-type spinon excitation in the lower band can form a magnetic polaron bound state at momentum $\mathbf{k}'$ with the chargon. This process is illustrated in Fig. 3(b) and corresponds to momentum and energy transfers $\mathbf{k}$ and $\omega = -\omega_s^+(\mathbf{k}) + \omega_{\mathrm{mp}}(\mathbf{k}')$. It readily explains why the lowest-energy spectral weight in Fig. 2 appears at $\mathbf{k} = (\pi, \pi)$, where $-\omega_s^+(\mathbf{k}) = \omega_s^-(\mathbf{k})$ becomes minimal, and for energies $\mathcal{O}(J)$ below $\omega^0_{\mathrm{mp}} = \min_{\mathbf{q}}(\omega_{\mathrm{mp}}(\mathbf{q}))$. A second type of process allowed for $T > 0$ starts from the same thermally excited spinon $\hat{f}^\dagger_{\mathbf{k}}$ in the upper band, which is deexcited by the ARPES beam. In this case it is assumed that the corresponding hole-type spinon excitation $\hat{f}_{\mathbf{k}'}$ in the lower band simultaneously scatters from $\mathbf{k}'$ to a final momentum $\mathbf{k}' + \Delta\mathbf{k}$. This is illustrated in Fig. 3(c) and implies momentum and energy transfers $\mathbf{k} + \Delta\mathbf{k}$ and $\omega = -\omega_s^+(\mathbf{k}) + \omega_{\mathrm{mp}}(\mathbf{k}' + \Delta\mathbf{k})$.

The single-hole ARPES spectrum is obtained as a convolution of the initial spinon and the final magnetic polaron states, combining all processes above and implying a broad spectral feature around $\mathbf{k} = (\pi, \pi)$ at finite temperature. However, additional maxima in the spectrum can emerge when taking into account the increased density of states of magnetic polarons at the edge of the magnetic BZ. This effect is particularly pronounced on the four-leg cylinder we study, where low-energy magnetic polarons with a high, quasi-one-dimensional density of states along k_x exist only at the inequivalent momenta $(\pi, 0)$, $(\pi/2, \pi/2)$, $(0, \pi)$, at similar energy ω^0_{mp}. Allowing only these final magnetic polaron momenta in the processes described in Fig. 3 yields three pronounced peaks observed around $\mathbf{k} = (\pi, \pi)$ in Fig. 2(b): the magnetic polaron at $T = 0$ (solid line) and the thermal spinon without (dashed) and with (dotted) scattering. The precise fit parameters we used in Fig. 2(b) are provided in the Supplemental Material [85]. The expected features are in good qualitative agreement with our numerically obtained spectra.

III. DISCUSSION AND OUTLOOK

The t-J model studied in this work, and the closely related Hubbard model, have been realized using ultracold atoms in optical lattices [53–56,99] as well as in Rydberg tweezer arrays [12], allowing for measurements of the single-hole ARPES spectrum [63,64,100]. The robustness of the quasiparticle peak we find in our spectra, up to $T \approx 2J$, i.e., well above the temperatures reached in state-of-the-art experiments [101], indicates that spectroscopic studies of magnetic polarons are well within reach.

A central result of our work is the prediction that low-energy spectral weight—notably absent at low temperatures—reappears outside the magnetic BZ as T increases. We explain this phenomenon by nearly-deconfined spinon excitations in the undoped Heisenberg AFM, which may also underlie Fermi-arc formation. We propose to test this hypothesis further by performing measurements at finite doping, or using pump-probe variants of ARPES [93]. By establishing how spectral weight reappears outside the magnetic BZ we hope to reveal the mechanism leading to its suppression at low T in the first place.

Although the temperature range $T = 0.25$–$2\,J$ explored in this work extends well above the low-temperature limit often associated with doped Mott insulators, it is directly relevant for both experimental and theoretical reasons. On the experimental side, similar temperatures are routinely achieved in quantum simulation platforms such as ultracold atoms and Rydberg arrays, where the dynamics of doped Mott systems can be probed with microscopic control. In addition, ARPES experiments on cuprate materials are typically conducted at finite temperatures corresponding to this scale. The persistence of polaron features up to $T \sim 2J$ thus points to their robustness, suggesting that such quasiparticles remain meaningful even when thermal fluctuations are substantial.

A natural next step is to extend our approach to compute spectral functions on top of a finite-doped, finite-temperature background. While conceptually straightforward, this presents significant numerical challenges due to increased entanglement and particle-number constraints. We leave this promising direction for future work.

Further possible extensions of our work include the study of Hubbard-Mott excitons [102,103], rotational one-hole excitations [47,104] or two-hole ARPES spectra [105,106] at finite temperatures. All these approaches will lead to a better

microscopic understanding of the emergent charge carriers of doped AFM Mott insulators in the strongly correlated regime, believed to constitute key ingredients of high-T_c superconductivity in cuprate compounds.

An interesting direction for future work is to explore how phase shifts associated with hole doping—such as those observed in the 1D Hubbard model [107] and proposed to generalize to $(\pm\pi/2, \pm\pi/2)$ in 2D [108]—might influence the spectral function. Our current mean-field framework does not explicitly incorporate such phase shifts, but the reemergence of spectral weight near (π, π) at finite temperature may reflect related underlying physics. Making this connection more precise could offer further insight into the momentum structure of magnetic polarons.

While Schwinger bosons provide a natural description of long-range antiferromagnetic order through spinon condensation, they are less suited for capturing the finite-temperature dynamics considered here. In particular, a bosonic spinon mean-field treatment tends to produce strong spectral weight at (0,0) or (π, π), inconsistent with numerical results [42]. By contrast, the fermionic spinon framework used in our study effectively models short-range AFM correlations and reproduces key spectral features such as the suppression of weight at (π, π). Going beyond mean-field theory, bosonic and fermionic approaches may become equivalent, but such treatments remain prohibitively difficult.

Complementary real-time and real-space dynamics of a single mobile hole in the two-dimensional t-J model at finite temperature are explored in a follow-up paper [109]. That work analyzes the hole's spreading behavior and associated spin correlations, providing insight into dynamical processes relevant for cold-atom experiments. Together, these studies offer a comprehensive picture of both spectral and dynamical properties of doped Mott insulators at finite temperature.

ACKNOWLEDGMENTS

The authors thank Sebastian Paeckel and Pit Bermes for helpful discussions. This work was funded in part by the Deutsche Forschungsgemeinschaft under Germany's Excellence Strategy EXC-2111 (Project No. 390814868). It is part of the Munich Quantum Valley, supported by the Bavarian state government with funds from the Hightech Agenda Bayern Plus. F.G. acknowledges funding from the European Research Council (ERC) under the European Union's Horizon 2020 Research and Innovation Program (Grant Agreement No. 948141) — ERC Starting Grant SimUcQuam.

DATA AVAILABILITY

The data that support the findings of this article are not publicly available upon publication because it is not technically feasible and/or the cost of preparing, depositing, and hosting the data would be prohibitive within the terms of this research project. The data are available from the authors upon reasonable request.

[1] G. R. Stewart, Heavy-fermion systems, Rev. Mod. Phys. **56**, 755 (1984).
[2] P. A. Lee, N. Nagaosa, and X.-G. Wen, Doping a Mott insulator: Physics of high-temperature superconductivity, Rev. Mod. Phys. **78**, 17 (2006).
[3] B. Keimer, S. A. Kivelson, M. R. Norman, S. Uchida, and J. Zaanen, From quantum matter to high-temperature superconductivity in copper oxides, Nature (London) **518**, 179 (2015).
[4] L. Bulaevskii, E. Nagaev, and D. Khomskii, A new type of auto-localized state of a conduction electron in an antiferromagnetic semiconductor, JETP, **836**, 27 (1968).
[5] S. A. Trugman, Interaction of holes in a Hubbard antiferromagnet and high-temperature superconductivity, Phys. Rev. B **37**, 1597 (1988).
[6] C. L. Kane, P. A. Lee, and N. Read, Motion of a single hole in a quantum antiferromagnet, Phys. Rev. B **39**, 6880 (1989).
[7] S. Sachdev, Hole motion in a quantum Néel state, Phys. Rev. B **39**, 12232 (1989).
[8] F. Ronning, K. M. Shen, N. P. Armitage, A. Damascelli, D. H. Lu, Z.-X. Shen, L. L. Miller, and C. Kim, Anomalous high-energy dispersion in angle-resolved photoemission spectra from the insulating cuprate $Ca_2CuO_2Cl_2$, Phys. Rev. B **71**, 094518 (2005).
[9] J. Graf, G.-H. Gweon, K. McElroy, S. Y. Zhou, C. Jozwiak, E. Rotenberg, A. Bill, T. Sasagawa, H. Eisaki, S. Uchida, H. Takagi, D.-H. Lee, and A. Lanzara, Universal high energy anomaly in the angle-resolved photoemission spectra of high temperature superconductors: Possible evidence of spinon and holon branches, Phys. Rev. Lett. **98**, 067004 (2007).
[10] J. Koepsell, J. Vijayan, P. Sompet, F. Grusdt, T. A. Hilker, E. Demler, G. Salomon, I. Bloch, and C. Gross, Imaging magnetic polarons in the doped Fermi-Hubbard model, Nature (London) **572**, 358 (2019).
[11] G. Ji, M. Xu, L. H. Kendrick, C. S. Chiu, J. C. Brüggenjürgen, D. Greif, A. Bohrdt, F. Grusdt, E. Demler, M. Lebrat, and M. Greiner, Coupling a mobile hole to an antiferromagnetic spin background: Transient dynamics of a magnetic polaron, Phys. Rev. X **11**, 021022 (2021).
[12] M. Qiao, G. Emperauger, C. Chen, L. Homeier, S. Hollerith, G. Bornet, R. Martin, B. Gély, L. Klein, D. Barredo, S. Geier, N.-C. Chiu, F. Grusdt, A.Bohrdt, T. Lahaye, and A. Browaeys, Realization of a doped quantum antiferromagnet in a Rydberg tweezer array, Nature (London) **644**, 889 (2025).
[13] A. Damascelli, Z. Hussain, and Z.-X. Shen, Angle-resolved photoemission studies of the cuprate superconductors, Rev. Mod. Phys. **75**, 473 (2003).
[14] S. A. Trugman, Spectral function of a hole in a Hubbard antiferromagnet, Phys. Rev. B **41**, 892 (1990).
[15] V. Elser, D. A. Huse, B. I. Shraiman, and E. D. Siggia, Ground state of a mobile vacancy in a quantum antiferromagnet: Small-cluster study, Phys. Rev. B **41**, 6715 (1990).
[16] G. Martinez and P. Horsch, Spin polarons in the t-J model, Phys. Rev. B **44**, 317 (1991).
[17] M. Boninsegni and E. Manousakis, Quasihole excitation in a quantum antiferromagnet: Variational Monte Carlo calculation, Phys. Rev. B **43**, 10353 (1991).
[18] Z. Liu and E. Manousakis, Spectral function of a hole in the t-J model, Phys. Rev. B **44**, 2414 (1991).

[19] P. Beran, D. Poilblanc, and R. Laughlin, Evidence for composite nature of quasiparticles in the 2D *t-J* model, Nucl. Phys. B **473**, 707 (1996).

[20] F. Grusdt, A. Bohrdt, and E. Demler, Microscopic spinon-chargon theory of magnetic polarons in the *t–J* model, Phys. Rev. B **99**, 224422 (2019).

[21] K. K. Nielsen, M. A. Bastarrachea-Magnani, T. Pohl, and G. M. Bruun, Spatial structure of magnetic polarons in strongly interacting antiferromagnets, Phys. Rev. B **104**, 155136 (2021).

[22] P. Bermes, A. Bohrdt, and F. Grusdt, Magnetic polarons beyond linear spin-wave theory: Mesons dressed by magnons, Phys. Rev. B **109**, 205104 (2024).

[23] K. Kurokawa, S. Isono, Y. Kohama, S. Kunisada, S. Sakai, R. Sekine, M. Okubo, M. D. Watson, T. K. Kim, C. Cacho, S. Shin, T. Tohyama, K. Tokiwa, and T. Kondo, Unveiling phase diagram of the lightly doped high-T_c cuprate superconductors with disorder removed, Nat. Commun. **14**, 4064 (2023).

[24] W. Chen, O. P. Sushkov, and T. Tohyama, Angle-resolved photoemission spectral function in lightly doped and antiferromagnetically ordered $YBa_2Cu_3O_{6+y}$, Phys. Rev. B **84**, 195125 (2011).

[25] B. Bacq-Labreuil, C. Fawaz, Y. Okazaki, Y. Obata, H. Cercellier, P. Le Fèvre, F. Bertran, D. Santos-Cottin, H. Yamamoto, I. Yamada, M. Azuma, K. Horiba, H. Kumigashira, M. d'Astuto, S. Biermann, and B. Lenz, Universal waterfall feature in cuprate superconductors: Evidence of a momentum-driven crossover, Phys. Rev. Lett. **134**, 016502 (2025).

[26] J. M. Hauschild, Quantum many-body systems far out of equilibrium—simulations with tensor networks, Ph.D. thesis, Technische Universität München, 2019.

[27] S. Paeckel, T. Köhler, A. Swoboda, S. R. Manmana, U. Schollwöck, and C. Hubig, Time-evolution methods for matrix-product states, Ann. Phys. **411**, 167998 (2019).

[28] J.-W. Li, A. Gleis, and J. von Delft, Time-dependent variational principle with controlled bond expansion for matrix product states, Phys. Rev. Lett. **133**, 026401 (2024).

[29] B. Dalla Piazza, M. Mourigal, N. B. Christensen, G. J. Nilsen, P. Tregenna-Piggott, T. G. Perring, M. Enderle, D. F. McMorrow, D. A. Ivanov, and H. M. Ronnow, Fractional excitations in the square-lattice quantum antiferromagnet, Nat. Phys. **11**, 62 (2015).

[30] E. Dagotto, A. Moreo, R. Joynt, S. Bacci, and E. Gagliano, Dynamics of one hole in the *t-J* model, Phys. Rev. B **41**, 2585 (1990).

[31] K. Hallberg, A. G. Rojo, and C. A. Balseiro, One-hole spectral densities in the polarized *t-J* model, Phys. Rev. B **43**, 8005 (1991).

[32] Z. Liu and E. Manousakis, Loop-expansion study of the single-hole spectral function in the *t-J* model, Phys. Rev. B **51**, 3156 (1995).

[33] Z. B. Su, Y. M. Li, W. Y. Lai, and L. Yu, Self-consistent renormalized hole motion in a quantum antiferromagnet, Phys. Rev. Lett. **63**, 1318 (1989).

[34] S. Schmitt-Rink, C. M. Varma, and A. E. Ruckenstein, Spectral function of holes in a quantum antiferromagnet, Phys. Rev. Lett. **60**, 2793 (1988).

[35] Z. Liu and E. Manousakis, Dynamical properties of a hole in a Heisenberg antiferromagnet, Phys. Rev. B **45**, 2425 (1992).

[36] K. K. Nielsen, T. Pohl, and G. M. Bruun, Nonequilibrium hole dynamics in antiferromagnets: Damped strings and polarons, Phys. Rev. Lett. **129**, 246601 (2022).

[37] N. G. Diamantis and E. Manousakis, Dynamics of string-like states of a hole in a quantum antiferromagnet: a diagrammatic Monte Carlo simulation, New J. Phys. **23**, 123005 (2021).

[38] P. W. Leung and R. J. Gooding, Dynamical properties of the single-hole *t-J* model on a 32-site square lattice, Phys. Rev. B **52**, R15711(R) (1995).

[39] P. W. Leung and R. J. Gooding, Erratum: Dynamical properties of the single-hole $t-J$ model on a 32-site square lattice, Phys. Rev. B **54**, 711(E) (1996).

[40] M. Brunner, F. F. Assaad, and A. Muramatsu, Single-hole dynamics in the $t-J$ model on a square lattice, Phys. Rev. B **62**, 15480 (2000).

[41] A. S. Mishchenko, N. V. Prokof'ev, and B. V. Svistunov, Single-hole spectral function and spin-charge separation in the $t-J$ model, Phys. Rev. B **64**, 033101 (2001).

[42] A. Bohrdt, E. Demler, F. Pollmann, M. Knap, and F. Grusdt, Parton theory of ARPES spectra in anti-ferromagnetic Mott insulators, Phys. Rev. B **102**, 035139 (2020).

[43] P. Wrzosek and K. Wohlfeld, Hole in the two-dimensional Ising antiferromagnet: Origin of the incoherent spectrum, Phys. Rev. B **103**, 035113 (2021).

[44] B. I. Shraiman and E. D. Siggia, Mobile vacancies in a quantum Heisenberg antiferromagnet, Phys. Rev. Lett. **61**, 467 (1988).

[45] E. Dagotto, R. Joynt, A. Moreo, S. Bacci, and E. Gagliano, Strongly correlated electronic systems with one hole: Dynamical properties, Phys. Rev. B **41**, 9049 (1990).

[46] E. Manousakis, String excitations of a hole in a quantum antiferromagnet and photoelectron spectroscopy, Phys. Rev. B **75**, 035106 (2007).

[47] F. Grusdt, M. Kánasz-Nagy, A. Bohrdt, C. S. Chiu, G. Ji, M. Greiner, D. Greif, and E. Demler, Parton theory of magnetic polarons: Mesonic resonances and signatures in dynamics, Phys. Rev. X **8**, 011046 (2018).

[48] S. Kar and E. Manousakis, Finite-temperature spectral function of a hole in a quantum antiferromagnet and the role of phonons, Phys. Rev. B **78**, 064508 (2008).

[49] F. C. Zhang and T. M. Rice, Effective Hamiltonian for the superconducting Cu oxides, Phys. Rev. B **37**, 3759 (1988).

[50] S. Jiang, D. J. Scalapino, and S. R. White, Ground-state phase diagram of the *t-t'-J* model, Proc. Natl. Acad. Sci. USA **118**, e2109978118 (2021).

[51] A. V. Gorshkov, S. R. Manmana, G. Chen, J. Ye, E. Demler, M. D. Lukin, and A. M. Rey, Tunable superfluidity and quantum magnetism with ultracold polar molecules, Phys. Rev. Lett. **107**, 115301 (2011).

[52] L. Homeier, T. J. Harris, T. Blatz, S. Geier, S. Hollerith, U. Schollwöck, F. Grusdt, and A. Bohrdt, Antiferromagnetic bosonic $t-J$ models and their quantum simulation in tweezer arrays, Phys. Rev. Lett. **132**, 230401 (2024).

[53] A. N. Carroll, H. Hirzler, C. Miller, D. Wellnitz, S. R. Muleady, J. Lin, K. P. Zamarski, R. R. W. Wang, J. L. Bohn, A. M. Rey, and J. Ye, Observation of generalized *t-J* spin dynamics with tunable dipolar interactions, Science **388**, 381 (2025).

[54] T. Esslinger, Fermi-Hubbard physics with atoms in an optical lattice, Annu. Rev. Condens. Matter Phys. **1**, 129 (2010).

[55] L. Tarruell and L. Sanchez-Palencia, Quantum simulation of the Hubbard model with ultracold fermions in optical lattices, C. R. Phys. **19**, 365 (2018).

[56] A. Bohrdt, L. Homeier, C. Reinmoser, E. Demler, and F. Grusdt, Exploration of doped quantum magnets with ultracold atoms, Ann. Phys. **435**, 168651 (2021), Special issue on Philip W. Anderson.

[57] R. Barends, L. Lamata, J. Kelly, L. García-Álvarez, A. G. Fowler, A. Megrant, E. Jeffrey, T. C. White, D. Sank, J. Y. Mutus, B. Campbell, Y. Chen, Z. Chen, B. Chiaro, A. Dunsworth, I.-C. Hoi, C. Neill, P. J. J. O'Malley, C. Quintana, P. Roushan *et al.*, Digital quantum simulation of fermionic models with a superconducting circuit, Nat. Commun. **6**, 7654 (2015).

[58] S. J. Evered, M. Kalinowski, A. A. Geim, T. Manovitz, D. Bluvstein, S. H. Li, N. Maskara, H. Zhou, S. Ebadi, M. Xu, J. Campo, M. Cain, S. Ostermann, S. F. Yelin, S. Sachdev, M. Greiner, V. Vuletić, and M. D. Lukin, Probing topological matter and fermion dynamics on a neutral-atom quantum computer, Nature (London) **645**, 341 (2025).

[59] C. Kollath, M. Köhl, and T. Giamarchi, Scanning tunneling microscopy for ultracold atoms, Phys. Rev. A **76**, 063602 (2007).

[60] T.-L. Dao, A. Georges, J. Dalibard, C. Salomon, and I. Carusotto, Measuring the one-particle excitations of ultracold fermionic atoms by stimulated Raman spectroscopy, Phys. Rev. Lett. **98**, 240402 (2007).

[61] T.-L. Dao, I. Carusotto, and A. Georges, Probing quasiparticle states in strongly interacting atomic gases by momentum-resolved Raman photoemission spectroscopy, Phys. Rev. A **80**, 023627 (2009).

[62] P. Törmä, Physics of ultracold Fermi gases revealed by spectroscopies, Phys. Scr. **91**, 043006 (2016).

[63] A. Bohrdt, D. Greif, E. Demler, M. Knap, and F. Grusdt, Angle-resolved photoemission spectroscopy with quantum gas microscopes, Phys. Rev. B **97**, 125117 (2018).

[64] P. T. Brown, E. Guardado-Sanchez, B. M. Spar, E. W. Huang, T. P. Devereaux, and W. S. Bakr, Angle-resolved photoemission spectroscopy of a Fermi-Hubbard system, Nat. Phys. **16**, 26 (2020).

[65] S. R. White, Density matrix formulation for quantum renormalization groups, Phys. Rev. Lett. **69**, 2863 (1992).

[66] S. R. White, Density-matrix algorithms for quantum renormalization groups, Phys. Rev. B **48**, 10345 (1993).

[67] U. Schollwöck, The density-matrix renormalization group in the age of matrix product states, Ann. Phys. **326**, 96 (2011).

[68] A. Nocera and G. Alvarez, Symmetry-conserving purification of quantum states within the density matrix renormalization group, Phys. Rev. B **93**, 045137 (2016).

[69] A. E. Feiguin and S. R. White, Finite-temperature density matrix renormalization using an enlarged Hilbert space, Phys. Rev. B **72**, 220401(R) (2005).

[70] A. E. Feiguin and G. A. Fiete, Spectral properties of a spin-incoherent Luttinger liquid, Phys. Rev. B **81**, 075108 (2010).

[71] J. J. García-Ripoll, Time evolution of matrix product states, New J. Phys. **8**, 305 (2006).

[72] P. E. Dargel, A. Wöllert, A. Honecker, I. P. McCulloch, U. Schollwöck, and T. Pruschke, Lanczos algorithm with matrix product states for dynamical correlation functions, Phys. Rev. B **85**, 205119 (2012).

[73] M. L. Wall, Out-of-equilibrium dynamics with matrix product states, in *Quantum Many-Body Physics of Ultracold Molecules in Optical Lattices* (Springer, Cham, Switzerland, 2015), pp. 177–222.

[74] J. Haegeman, J. I. Cirac, T. J. Osborne, I. Pižorn, H. Verschelde, and F. Verstraete, Time-dependent variational principle for quantum lattices, Phys. Rev. Lett. **107**, 070601 (2011).

[75] J. Haegeman, C. Lubich, I. Oseledets, B. Vandereycken, and F. Verstraete, Unifying time evolution and optimization with matrix product states, Phys. Rev. B **94**, 165116 (2016).

[76] C. Karrasch, J. H. Bardarson, and J. E. Moore, Finite-temperature dynamical density matrix renormalization group and the Drude weight of spin-1/2 chains, Phys. Rev. Lett. **108**, 227206 (2012).

[77] D. Kennes and C. Karrasch, Extending the range of real time density matrix renormalization group simulations, Comput. Phys. Commun. **200**, 37 (2016).

[78] C. Karrasch, J. Bardarson, and J. Moore, Reducing the numerical effort of finite-temperature density matrix renormalization group calculations, New J. Phys. **15**, 083031 (2013).

[79] A. Gleis, J.-W. Li, and J. von Delft, Controlled bond expansion for density matrix renormalization group ground state search at single-site costs, Phys. Rev. Lett. **130**, 246402 (2023).

[80] A. Weichselbaum, Non-Abelian symmetries in tensor networks: A quantum symmetry space approach, Ann. Phys. **327**, 2972 (2012).

[81] A. Weichselbaum, X-symbols for non-Abelian symmetries in tensor networks, Phys. Rev. Res. **2**, 023385 (2020).

[82] A. Weichselbaum, QSpace – An open source tensor library for Abelian and non-Abelian symmetries, SciPost Phys. Codebases **40** (2024).

[83] B. J. Leland, *Digital Filters and Signal Processing* (Kluwer Academic Publishers, Boston, 1989).

[84] R. Verresen, F. Pollmann, and R. Moessner, Quantum dynamics of the square-lattice Heisenberg model, Phys. Rev. B **98**, 155102 (2018).

[85] See Supplemental Material at http://link.aps.org/supplemental/10.1103/4588-hpc2 for additional data and information regarding the simulation.

[86] N.-E. Guenther, P. Massignan, M. Lewenstein, and G. M. Bruun, Bose polarons at finite temperature and strong coupling, Phys. Rev. Lett. **120**, 050405 (2018).

[87] A. Mazurenko, C. S. Chiu, G. Ji, M. F. Parsons, M. Kanasz-Nagy, R. Schmidt, F. Grusdt, E. Demler, D. Greif, and M. Greiner, A cold-atom Fermi-Hubbard antiferromagnet, Nature (London) **545**, 462 (2017).

[88] K. M. Shen, F. Ronning, D. H. Lu, F. Baumberger, N. J. C. Ingle, W. S. Lee, W. Meevasana, Y. Kohsaka, M. Azuma, M. Takano, H. Takagi, and Z.-X. Shen, Nodal quasiparticles and antinodal charge ordering in $Ca_{2-x}Na_xCuO_2Cl$, Science **307**, 901 (2005).

[89] B. J. Kim, H. Koh, E. Rotenberg, S.-J. Oh, H. Eisaki, N. Motoyama, S. Uchida, T. Tohyama, S. Maekawa, Z.-X. Shen, and C. Kim, Distinct spinon and holon dispersions in photoemission spectral functions from one-dimensional $SrCuO_2$, Nat. Phys. **2**, 397 (2006).

[90] K. J. von Szczepanski, P. Horsch, W. Stephan, and M. Ziegler, Single-particle excitations in a quantum antiferromagnet, Phys. Rev. B **41**, 2017 (1990).

[91] R. Eder and Y. Ohta, Photoemission spectra of the t-J model in one and two dimensions: Similarities and differences, Phys. Rev. B **56**, 2542 (1997).

[92] R. N. Bannister and N. d'Ambrumenil, Spectral functions of half-filled one-dimensional Hubbard rings with varying boundary conditions, Phys. Rev. B **61**, 4651 (2000).

[93] A. Schuckert, A. Bohrdt, E. Crane, and F. Grusdt, Visualizing spinon Fermi surfaces with time-dependent spectroscopy, Phys. Rev. B **104**, 235107 (2021).

[94] M. Kohno, Mott transition in the two-dimensional Hubbard model, Phys. Rev. Lett. **108**, 076401 (2012).

[95] M. Charlebois and M. Imada, Single-particle spectral function formulated and calculated by variational Monte Carlo method with application to d-wave superconducting state, Phys. Rev. X **10**, 041023 (2020).

[96] T. K. Lee and S. Feng, Doping dependence of antiferromagnetism in La_2CuO_4: A numerical study based on a resonating-valence-bond state, Phys. Rev. B **38**, 11809 (1988).

[97] N. Trivedi and D. M. Ceperley, Green-function Monte Carlo study of quantum antiferromagnets, Phys. Rev. B **40**, 2737 (1989).

[98] C. Reinmoser, M. Xu, L. H. Kendrick, A. Kale, Y. Gang, M. Lebrat, M. Greiner, F. Grusdt, and A. Bohrdt, Optimized Gutzwiller projected states for doped antiferromagnets in Fermi-Hubbard simulators, arXiv:2506.11227.

[99] A. Bohrdt, D. Wei, D. Adler, K. Srakaew, S. Agrawal, P. Weckesser, I. Bloch, F. Grusdt, and J. Zeiher, Microscopy of bosonic charge carriers in staggered magnetic fields, arXiv:2410.19500.

[100] K. K. Nielsen, M. Zwierlein, and G. M. Bruun, Dual spectroscopy of quantum simulated Fermi-Hubbard systems, Phys. Rev. Lett. **135**, 043401 (2025).

[101] M. Xu, L. H. Kendrick, A. Kale, Y. Gang, C. Feng, S. Zhang, A. W. Young, M. Lebrat, and M. Greiner, A neutral-atom Hubbard quantum simulator in the cryogenic regime, Nature (London) **642**, 909 (2025).

[102] T.-S. Huang, C. L. Baldwin, M. Hafezi, and V. Galitski, Spin-mediated Mott excitons, Phys. Rev. B **107**, 075111 (2023).

[103] A. Bohrdt, E. Demler, and F. Grusdt, Spectroscopy of Hubbard-Mott excitons and their ro-vibrational excitations, arXiv:2406.16854.

[104] A. Bohrdt, E. Demler, and F. Grusdt, Rotational resonances and Regge-like trajectories in lightly doped antiferromagnets, Phys. Rev. Lett. **127**, 197004 (2021).

[105] F. Grusdt, E. Demler, and A. Bohrdt, Pairing of holes by confining strings in antiferromagnets, SciPost Phys. **14**, 090 (2023).

[106] A. Bohrdt, E. Demler, and F. Grusdt, Dichotomy of heavy and light pairs of holes in the t-J model, Nat. Commun. **14**, 8017 (2023).

[107] Y. Ren and P. W. Anderson, Asymptotic correlation functions in the one-dimensional Hubbard model with applications to high-T_c superconductivity, Phys. Rev. B **48**, 16662 (1993).

[108] D. N. Sheng, Y. C. Chen, and Z. Y. Weng, Phase string effect in a doped antiferromagnet, Phys. Rev. Lett. **77**, 5102 (1996).

[109] T. Guthardt, M. Scheb, J. von Delft, F. Grusdt, and A. Bohrdt, following paper, Finite-temperature real-time properties of magnetic polarons in two-dimensional quantum antiferromagnets, Phys. Rev. B **112**, 205118 (2025).